This article was downloaded by: [Tomsk State University of Control Systems and Radio]
On: 19 February 2013, At: 11:56
Publisher: Taylor & Francis
Informa Ltd Registered in England and Wales Registered Number: 1072954 Registered office: Mortimer House, 37-41 Mortimer Street, London W1T 3JH, UK

Molecular Crystals and Liquid Crystals Incorporating Nonlinear Optics

Publication details, including instructions for authors and subscription information:
http://www.tandfonline.com/loi/gmcl17

Spatial Extension of Charge Traps: Consequences for Space-Charge-Limited Currents

J. Kalinowski [a] , J. Godlewski [a] & P. Mondalski [a]

[a] Department of Molecular Physics, Technical University of Gdansk, 80-952, Gdansk, Poland

Version of record first published: 22 Sep 2006.

To cite this article: J. Kalinowski , J. Godlewski & P. Mondalski (1989): Spatial Extension of Charge Traps: Consequences for Space-Charge-Limited Currents, Molecular Crystals and Liquid Crystals Incorporating Nonlinear Optics, 175:1, 67-83

To link to this article: http://dx.doi.org/10.1080/00268948908033747

PLEASE SCROLL DOWN FOR ARTICLE

Full terms and conditions of use: http://www.tandfonline.com/page/terms-and-conditions

This article may be used for research, teaching, and private study purposes. Any substantial or systematic reproduction, redistribution, reselling, loan, sub-licensing, systematic supply, or distribution in any form to anyone is expressly forbidden.

The publisher does not give any warranty express or implied or make any representation that the contents will be complete or accurate or up to date. The accuracy of any instructions, formulae, and drug doses should be independently verified with primary sources. The publisher shall not be liable for any loss, actions, claims, proceedings, demand, or costs or damages whatsoever or howsoever caused arising directly or indirectly in connection with or arising out of the use of this material.

Mol. Cryst. Liq. Cryst., 1989, Vol. 175, pp. 67–83
Reprints available directly from the publisher
Photocopying permitted by license only
© 1989 Gordon and Breach Science Publishers S.A.
Printed in the United States of America

Downloaded by [Tomsk State University of Control Systems and Radio] at 11:56 19 February 2013

Spatial Extension of Charge Traps: Consequences for Space-Charge-Limited Currents†

J. KALINOWSKI, J. GODLEWSKI and P. MONDALSKI

Department of Molecular Physics, Technical University of Gdańsk, 80-952 Gdańsk, Poland

(*Received October 20, 1988*)

It is proposed that charge carriers are trapped by spatially extended domains (macrotraps) produced by physical perturbations of crystal lattice. These extended domains consist of local traps (microtraps) with energy (E) distributed in space (r) such that $E = (3kT/\sigma)\ln(r_o/r)$, where σ is a characteristic parameter of the exponential energy distribution function, and r_o is the radius of the macrotrap. The steady-state space-charge-limited currents (SCLC) are studied and interpreted by invoking the macrotrap concept. The results indicate that the potential of the macrotraps can be effectively modulated by an external electric field accessible in experiment and from the power law $j \sim U^n$ ($n > 2$) of the measured current (j versus voltage (U) σ can be determined ($n = 2 + 3/\sigma$). In particular, we examined high-quality anthracene crystals for which two distinct distributions of microtraps have been found with $\sigma_1 = 1 \pm 0.2$ and $\sigma_2 = 0.3 \pm 0.05$. Typical values of the concentration $N_o = 10^{15}\text{cm}^{-3}$ and depth $E_t = 0.6 \pm 0.05\text{eV}$ of macrotraps are accompanied by a diversity of r_o within the range $100\text{Å} < r_o < 10^3\text{Å}$.

PACS numbers: 72.20.Jv; 72.80.Le; 72.80.Sk

I. INTRODUCTION

The development of modern electronics has motivated work on electrical properties of every now and again new insulating and semiconducting materials among which molecular materials become of particular interest. The steady-state transport properties of charge carriers in such materials are often dominated by the presence and distribution of carrier trapping sites (charge traps) (e.g. References 1,2). Traps of either chemical or physical nature may be located at specific lattice sites (point defects) or possess an extended character (e.g. linear or planar defects or faults) (see e.g. Reference 3). SCLC flow through insulating crystals is often used to calculate trap parameters based on the assumption that the energy distribution of traps can be described by either exponential[2,4,5] or Gaussian function[3] with infinite limit of trap energies and homogeneous distribution in space (Figure 1A). This approach seems to be unrealistic and leads to well known discrepancies with ther-

†Dedicated to Prof. Martin Pope on the occasion of his 70th birthday.

Downloaded by [Tomsk State University of Control Systems and Radio] at 11:56 19 February 2013

mally stimulated current (TSC)[6-11] and thermoluminescence (TL)[12-18] studies which have generally indicated the presence of a discrete trap level. Though the discrete trap level has also been assumed to explain experimental SCLC j-U characteristics,[19,20] an apparent conflict appears when the density of traps is determined based on the temperature dependence of the trapping factor (θ) and that calculated from the trap-filled limit voltage (U_{TFL}).[2] There have been some attempts to explain the data in a unified manner. For example SCL hole currents in anthracene crystals have been interpreted based on exponential trap distributions produced by physical perturbations introduced by the same impurities which give rise to the discrete hole trap level as revealed by TSC studies.[21] Various concepts of local states of Gaussian distribution have been used to numerical fit of the theory to existing experimental j-U data.[22-24] However, none of the previous theories takes into account the essential physical factor of spatial extension of effective traps. In the present paper we go beyond the traditional approach and propose a physical interpretation of the SCLC flow arising from a trap model based on the concept that the whole population of traps can be divided into spatially extended domains (defected regions ≡ macrotraps), each macrotrap containing many localized states (microtraps) with energy distributed continuously according to a function decreasing with the distance (r) from the deepest state (E_t) standing for the macrotrap center. The energy (E) distribution of microtraps within a macrotrap, arises from specific metastable intermolecular conformations different from the molecular arrangement in the perfect

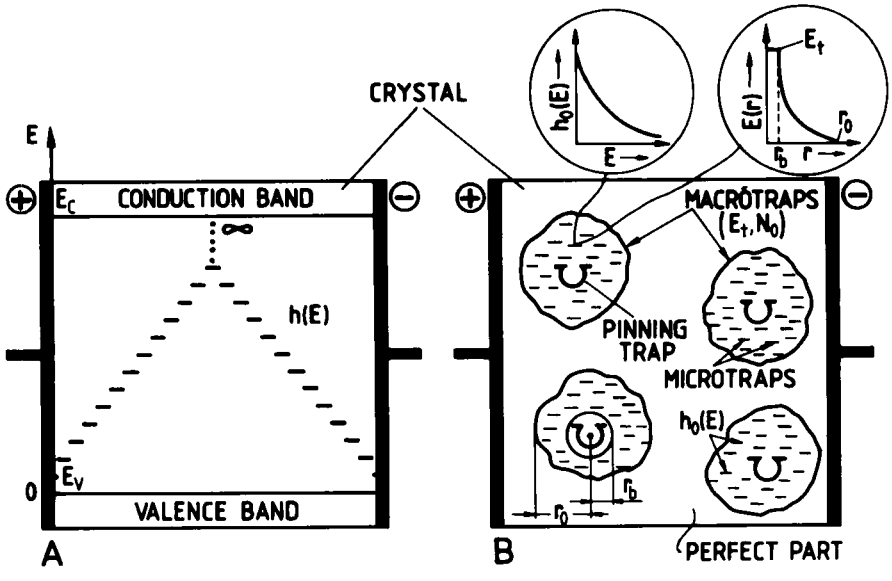

FIGURE 1 Schematic illustrating hole trap distributions in an insulating crystal placed in an electric field. A : homogeneous distribution in space with energy distribution function $h(E)$ over the whole bulk of the crystal; B : microtrap clusters pinned down on discrete macrotraps of various size r_t, and depth E_t. Microtraps are homogenously distributed within macrotraps and are characterized by energy distribution $h_o(E)$ and $E(r)$. Note that the energy distributions of microtraps are limited by the macrotrap depth E_t.

parts of the crystal and at a given temperature can be established by statistical thermodynamic arguments as an exponential function. Note that applying thermodynamic arguments to specific molecular conformations in a crystal favors the exponential distribution rather than pure statistical Gaussian function. The latter may be more realistic in a molecular random systems like amorphous organic films (see e.g. Reference 25). Therefore, choice of the exponential distribution is here not a matter of taste, but a consequence of the subject to be analyzed.

In the present work we establish criteria for the model to be applicable, and to illustrate the model, measurements of SCLC j-U characteristics on anthracene single crystals are carried out and quantitative discussion of the results presented.

II. THE MODEL OF TRAPS

A. Discrete set of macrotraps

In the following, we shall assume that the whole population of traps can be divided into a set of extended domains (macrotraps), each macrotrap consists of local traps (microtraps) distributed and limited in energy and space as illustrated in Figure 1B. Owing to a lack of detailed knowledge of such a cluster structure, we assume that macrotraps are in average spherical-symmetry cages of radius r_o, distributed in a random manner throughout the whole bulk of a crystalline sample.

If we let N_o denote the concentration of one type of macrotrap, H_o—the concentration of microtraps distributed in energy according to the exponential function

$$h_o(E) = \frac{H_o\sigma}{kT} \exp(-\sigma E/kT), \tag{1}$$

then the equation

$$h_o(E)dE = -4\pi r^2 N_m N_o dr \tag{2}$$

yields by definition the energy of microtraps as a function of distance (r) from the center of the macrotrap,

$$E(r) = \frac{3kT}{\sigma} \ln \frac{r_o}{r}. \tag{3}$$

The following integrating of (2)

$$\int_{\infty}^{0} h_o(E)\, dE = N_o \int_0^{r_o} N_m\, 4\pi r^2\, dr$$

gives

$$r_o = \left(\frac{3 H_o}{4\pi N_o N_m}\right)^{1/3} \tag{4}$$

Downloaded by [Tomsk State University of Control Systems and Radio] at 11:56 19 February 2013

and distribution (3) is assumed to be a quasi-continuous function, i.e. fulfilling the inequality

$$\left(\frac{dE}{dr}\right)\cdot a < kT, \tag{5}$$

where a is the lattice constant. Note that N_m in (2) and (4) is the molecular concentration identified with the effective density of states within a macrotrap [cf. (27)].

With general positional energy distribution (3), the microtrap depths are limited by the boundary conditions

$$E = 0 \quad \text{for} \quad r = r_o \tag{6}$$

and

$$E = E_t \quad \text{for} \quad r = r_b,$$

where r_b stands for the dimension of the basal pinning traps.

Since each macrotrap introduces its characteristic parameters r_o, r_b and σ, the total energy spectrum $h(E)$ of charge carrier trapping states is given by summing the density $h_o(E)$ over all macrotraps, i.e.

$$h(E) = \sum_i h_{oi}(E) \tag{7}$$

and the total concentration of microtraps $H = \sum_i H_{oi}$.

Expression (3) can be treated as a functional form of the attractive potential ($\phi = E/e$) for a charge e in the neutral macrotrap. This potential can be affected by an external electric field (F) lowering the trap potential barrier.[26,27] Using the distribution (3), the hole's (e) potential energy $V(r)$ with the field orientation ϑ is

$$V(r) = E(r) + eFr\cos\vartheta. \tag{8}$$

The potential energy maximum

$$V_{\max} = \frac{3kT}{\sigma}\left(1 + \ln\frac{r_o}{r_m}\right) \tag{9}$$

in the field direction is at

$$r_m = \frac{3kT}{\sigma eF\cos\vartheta}, \tag{10}$$

Downloaded by [Tomsk State University of Control Systems and Radio] at 11:56 19 February 2013

and the field lowering of the potential barrier is

$$\Delta E_H = \frac{3kT}{\sigma}\left[1 + \ln\left(\frac{eFr_o\sigma\cos\vartheta}{3kT}\right)\right] \tag{11}$$

for high fields such that $r_m < r_o$.

On the other hand, for low fields fulfilling condition $r_m \cong r_o$, we get simply

$$\Delta E_L = eFr_o. \tag{12}$$

The solid line of Figure 2 represents the potential energy of a hole in a neutral macrotrap in the absence of the applied electric field, and the dashed lines correspond to the potential in the presence of the applied field for two limiting cases of low and high electric fields.

If we assume the probability of hole escape from the trap to be governed by simple thermal excitation over the barrier, its value in the presence of the field is then increased to

$$\exp(-E_t/kT)\exp(\Delta E/kT), \tag{13}$$

which related to the attempt-to-escape rate (ν_{th}) gives the detrapping rate

$$\nu_L = \nu_{\text{th}}\exp(-E_t/kT)\cdot\exp(eFr_o/kT) \tag{14}$$

in the low-field approximation, and

$$\nu_H = \gamma F^{3/\sigma}\exp(-E_t/kT) \tag{15}$$

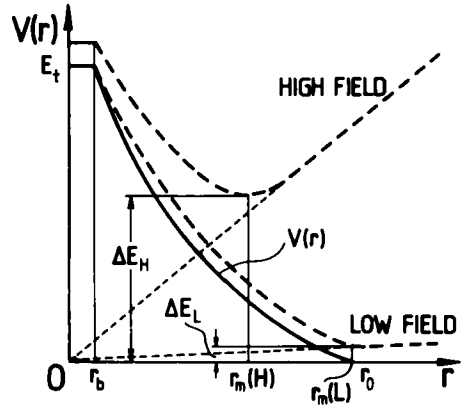

FIGURE 2 Schematic of a barrier for a hole in a neutral macrotrap being lowered by the applied field (for a more detailed description see text).

Downloaded by [Tomsk State University of Control Systems and Radio] at 11:56 19 February 2013

in the high-field approximation, where

$$\gamma = \nu_{th}\left(\frac{2.7er_o\sigma\cos\vartheta}{3kT}\right)^{3/\sigma}. \tag{16}$$

The analysis of SCLC flow will be based on the relations (14) and (15) in Sec.III.A.

B. Other distributions of macrotraps

If macrotraps are a product of random formation processes then for a phenomenological description of their energy (E_t) spectrum, a Gaussian approximation would be the most adequate,

$$N(E_t) = \frac{N_o}{2\pi\ \Delta_t}\exp(-E_t^2/2\Delta_t^2), \tag{17}$$

where Δ_t is the dispersion parameter related to the valence band edge.

However, macrotraps can be subject to other formation and distribution rules than pure statistical randomization; the deviations from the order being caused by thermodynamical and other physical and chemical factors acting primarily during crystal growth.

The exponential distribution of their energies might be then of importance,

$$N(E_t) = \frac{N_o}{l\ kT}\exp(-E_t/lkT), \tag{18}$$

where l is a parameter characteristic of the distribution. At considerable macrotrap densities (N_o) a statistical process of aggregation of macrotraps takes place, and formation of assemblies sets in. It is particularly effective when the mean distance between macrotraps is smaller than their double r_o

$$(N_o)^{-1/3} < 2r_o. \tag{19}$$

Interacting macrotraps can form a very complicated configuration of point defects (microtraps). Such a trap ensembles can consist of regions of compression and dilation of the lattice with a rather complicated energy spectrum in the inter-macrotrap regions. The resulted trap energy distribution depends upon an overlap between various type of macrotraps and, in general, the composite distribution function is not a simple linear combination of the component distributions corresponding to isolated macrotraps as given by Equation (7). If we assume the trapping levels to be reflecting the distribution of local stress fields, then, even for the defects described by the Gaussian distribution, as shown for dislocations generated at random,[28] there is considerable deflection from the normal distribution. This means that at random disposition of macrotraps, the stress field components of a macrotrap ensemble can create strong local fluctuations of stress at the tail end of

Downloaded by [Tomsk State University of Control Systems and Radio] at 11:56 19 February 2013

the Gaussian distribution; they in turn, can be the source of formation of deep structural traps for charge carriers.

For a large number of macrotraps the microtrap distributions can merge into a quasi-continuous exponential energy distribution with limiting energies determined by either macrotrap distribution (17) or (18).

Downloaded by [Tomsk State University of Control Systems and Radio] at 11:56 19 February 2013

III. STEADY-STATE ONE-CARRIER SCLC FLOW

The equations relating a unipolar (hole) injection drift current j, free n_f and trapped n_t charge carrier concentrations, internal electric field F, and the voltage U applied to the sample of thickness d for one-dimensional system are, in general, as follows:

$$j = e\, n_f(x)\, \mu(F)\, F(x), \tag{20}$$

$$\frac{dF(x)}{dx} = \frac{e}{\epsilon\, \epsilon_o}\, n(x), \tag{21}$$

$$U = \int_0^d F(x)dx, \tag{22}$$

$$n_f = n_f(n,x), \tag{23}$$

Here μ is the carrier mobility, ϵ is the dielectric constant, ϵ_o is the permittivity of free space, and the total concentration of charge $n = n_f + n_t$.

The solution of Equations (20)–(23) for ohmic contacts (SCLC) has been obtained by several authors (see References 1–5 and 29, 30) in different ways dependent on the value of the ratio $\theta = n_f/n$ and the functional shape of relation (23). The latter can be obtained from the principle of detailed balance, the trap filling and emptying rates must be equal in the steady state. This gives

$$\nu n_t = v\, s\, n_f(N_o - n_t), \tag{24}$$

where $[vs(N_o - n_t)]^{-1} = \tau =$ trapping time, s is the cross section of capture of a hole by a trap, N_o is the concentration of discrete traps, and v is the thermal velocity of the hole.

The relationship between n_f and n_t takes various forms dependent on the functional shape of the emptying rate which reflects characteristic features of the trap distributions. We now consider the derivation of j on the applied voltage with selected cases of the trap model described in Section II.

A. Solution for SCLC: discrete set of macrotraps

We can now derive the j-U dependence for the SCLC by solving Equations (20)–(23) with the filling-emptying balance (24) based upon the emptying rate given

either by Equation (14) or (15). In the high-field approximation the balance is

$$\gamma F^{3/\sigma} \exp(E_t/kT)\, n_t = vsn_f(N_o - n_t). \tag{25}$$

Assuming $n_f \ll n_t$, $n_t \ll N_o$, and $\vartheta = 0$, the system of Equations (20)–(22) and (25) can be solved and under SCLC conditions yields

$$j = \frac{N_{\text{eff}}}{N_o} \frac{\epsilon\epsilon_o\mu\sigma}{2\sigma + 3} \left(\frac{2.7er_o\sigma}{3kT}\right)^{3/\sigma} \left(\frac{3\sigma + 3}{2\sigma + 3}\right)^{2+3/\sigma} \exp(-E_t/kT)\, \frac{U^{2+3/\sigma}}{d^{3+3/\sigma}}, \tag{26}$$

where

$$N_{\text{eff}} = \nu_{\text{th}}/vs = (2\pi r_o^3)^{-1} \tag{27}$$

stands for the effective density of states in the crystal. The relation between N_{eff} and r_o has been obtained under the assumption that ν_{th} corresponds to the collision frequency of the trapped carrier with the potential barrier of the trap [$\nu_{\text{th}} = (2\tau)^{-1}$, where $\tau = r_o/v$] and $s = \pi r_o^2$.

If notion of the trapping factor

$$\theta = \frac{n_f}{n_t} = \frac{N_{\text{eff}}}{N_o} \left(\frac{2.7er_o\sigma}{3kT}\right)^{3/\sigma} \left(\frac{U}{d}\right)^{3/\sigma} \exp(-E_t/kT) \tag{28}$$

is introduced to the current description, then from Equation (26) it follows that j-U expression will be

$$j = \frac{\epsilon\epsilon_o\mu\sigma}{2\sigma + 3} \left(\frac{3\sigma + 3}{2\sigma + 3}\right)^{2+3/\sigma} \theta\, \frac{U^2}{d^3}. \tag{29}$$

The conductivity and j-U characteristic given by (29) can be, therefore, described as SCLC flow with field-dependent θ, the formulation similar to the Poole-Frenkel effect on space-charge-limited currents.[31,32] Such a situation is clearly not expected in the case of the standard Mark-Helfrich solution for trapping by a discrete set of separated microtraps,[29,30]

$$j = \frac{9}{8} \epsilon\, \epsilon_o\, \mu\, \theta\, \frac{U^2}{d^3}. \tag{30}$$

This is the case if one extrapolates Equation (26) to $\sigma \to \infty$, with

$$\theta = \frac{N_{\text{eff}}}{N_o} \exp(-E_t/kT). \tag{31}$$

The physical meaning of this extrapolation is that we deal with one discrete trap level (E_t), the trap potential being the infinitely sharp point well for which the barrier lowering can be neglected [$\Delta E_H \to 0$; see Equation (11)].

Downloaded by [Tomsk State University of Control Systems and Radio] at 11:56 19 February 2013

Since $\Delta E_L \rightarrow 0$ for low fields, Equations (30) and (31) stand as well for the solution in the low field approximation with v_L given by (14) for $eFr_o << kT$.

We note that the functional form of Equation (26) $j \sim U^n/d^m$ with $n > 2$ and $m > 3$, except for the constant coefficients, is in fact, identical to the SCL j-U characteristics for a continuous exponential distribution of the form (18) of the infinitely sharp well (ISW) point traps,[5]

$$j = \frac{N_{\text{eff}} e\mu}{H^l} \left(\frac{\epsilon\epsilon_o}{e}\right)^l \left[\frac{l^2 \sin(\pi/l)}{(l+1)\pi}\right]^l \left(\frac{2l+1}{l+1}\right)^{l+1} \frac{U^{l+1}}{d^{2l+1}}. \tag{32}$$

It follows, then, that experimental data arising from the discrete macrotrap background can, without close scrutiny, be mistakenly attributed to the continuous exponential distribution of ISW point traps.

The transition from the low- to high-field regions of the current occurs at a voltage

$$U_{tr}^{(\alpha)} = \frac{3kTd}{2.7er_o\sigma} \left(\frac{9}{8\sigma}\right)^{\sigma/3} \frac{(2\sigma+3)^{1+\sigma}}{(3\sigma+3)^{1+(2/3)\sigma}}, \tag{33}$$

which, having σ from $\log j - \log U$ slope, allows macrotrap dimension r_o to be determined.

From the above discussion, it is evident that the experimental form of j-U curves is not sufficient to unambiguously identify of the trap distribution underlying the SCLC flow. Even the steep rise in the current with increasing voltage, typically associated with the trap-filled limit, is not unambiguous, as it can be due to the voltage $U_{tr}^{(\beta)}$ which lowers the macrotrap barrier at the $r_m(\beta)$, where the microtrap distribution changes steeply its σ from the actual value σ_1 to σ_2.

B. Solution for SCLC: exponential distribution of macrotraps

Assuming the macrotraps to be distributed in eneregy according to (18), we can solve Equations. (20)–(23) and the result is then as follows:

$$j = \frac{N_{\text{eff}} e\mu}{N_o} \left(\frac{2.7er_o\sigma}{3kT}\right)^{3/\sigma} \left[\frac{\epsilon\epsilon_o \sin(\pi/l)}{e\,\pi\,N_o}\right]^1 \frac{[2 + (1 + 3/\sigma)(1/l)]^{1+l+3/\sigma}}{[1 + (1 + 3/\sigma)(1/l)]^{1+2l+3/\sigma}} \frac{U^{1+l+3/\sigma}}{d^{1+2l+3/\sigma}}. \tag{34}$$

For large σ ($\sigma \rightarrow \infty$), Equation (34) becomes identical with (32) that is reduces to the form characteristic for the continuous exponential distribution of ISW point traps.

IV. COMPARISON WITH EXPERIMENT AND DISCUSSION

A large number of experimental studies were carried out on SCLC flow in organic molecular crystals (see e.g. References 1–3 and references quoted therein). The

Downloaded by [Tomsk State University of Control Systems and Radio] at 11:56 19 February 2013

shapes of j-U characteristics are usually displayed in a log − log scale, showing typically 2 or 3 straight line segments attributed to diffusion currents in the low-voltage region and drift currents in the higher-voltage region. The drift currents have been interpreted in terms of an exponential or Gaussian model of ISW point traps.

It is well known that concentration and distribution of traps varies from crystal to crystal even then, when they are produced by cutting from a common boule or originate from a common amount of starting material crystallizing by evaporation or growing in solution. Thus the results obtained by us with solution grown anthracene single crystals are by no means universal for the whole class of organic crystals and differ from some other results reported for anthracene crystals. We have chosen solution grown crystals because they show less variation in trap parameters.[21,33] Ohmic CuI-hole injecting contacts were formed on the crystallographic ab-plane of the crystals. Figure 3 shows typical hole j-U characteristics for two of over 20 examined crystals. The current depends on voltage according to $j \sim U^n$ with $n > 2$ within the current range exceeding 8 decades, and the field range extended about 2 decades. This broad range of the both variables allows to yield substantial information about the concentration and distribution of traps. First the trap parameters were obtained by using the traditional equation (32) based on the quasi-continuous exponential distribution of ISW point traps. Table I lists the values of H and l obtained for hole traps in these two crystals.

Whereas the lowest field regions can be ascribed to the near-Child's law in the presence of shallow trapping, the consecutive straight-line segments should be

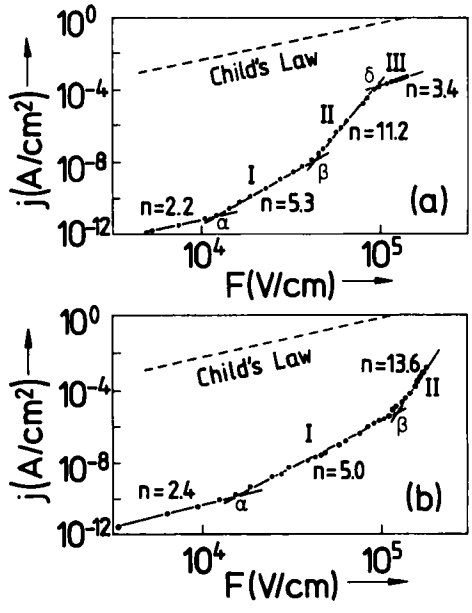

FIGURE 3 Current density as a function of electric field for two of over twenty examined solution-grown anthracene crystals at room temperature. Electrodes: copper iodide (CuI); crystal thickness: d = 66μm (a), d = 49μm (b).

Downloaded by [Tomsk State University of Control Systems and Radio] at 11:56 19 February 2013

TABLE I

Trapping parameters according to standard description by the exponential trap distribution model (32).

Regions \ Parameters	d = 66 μm		d = 49 μm	
	l	H (cm $^{-3}$)	l	H (cm $^{-3}$)
Region I	4.3	3.3×10^{19}	4.0	9×10^{19}
Region II	10.2	1.7×10^{17}	12.6	1.3×10^{17}
Region III	2.4	1×10^{21}	—	—

Downloaded by [Tomsk State University of Control Systems and Radio] at 11:56 19 February 2013

interpreted as follows: I—filling exponentially distributed trapping states: II—trap-filled limit; III—electrode-limited current. From the trap filled-limit voltage U_{TFL} for both crystals $N_t \approx 10^{13}\text{cm}^{-3}$ and the limiting Fermi energy can be calculated as $E_F = lkT\ln(H/N_t) \approx 1.4\text{eV}$.[30] Thus $n_f = N_{\text{eff}} \exp(-E_F/kT)$ gives $n_f \sim 10^{-3}\text{cm}^{-3}$ with $N_{\text{eff}} = 4 \times 10^{21}\ \text{cm}^{-3}$ and $kT = 0.025\text{eV}$. This value of n_f introduced to the current expression (20) with $\mu \sim 1\ \text{cm}^2/\text{Vs}$ and $F \sim 10^4\text{V/cm}$, leads to the current $j \sim 10^{-18}\text{A/cm}^2$, which is six orders of magnitude less than the experimental value. Another possibility of interpretation of the sharp change in the slope of the plot $\log j - \log F$ is sweeping of the quasi-Fermi level through exponentially distributed ISW point traps with different l. Then, at the transition voltage β (see Figure 3) $(H_1/lkT)\exp(-E_{tr}/l_1kT) = (H_2/l_2kT)\exp(-E_{tr}/l_2kT)$, and the average value for both crystals $E_{tr} = 1.14\text{eV}$ gives $n_f = 60\ \text{cm}^{-3}$. With this value of n_f and $F = 10^5$ V/cm one obtains $j \sim 10^{-12}\ \text{A/cm}^2$, which is four orders of magnitude less than the experimental result.

The above discrepancies indicate that the sharp changes in the slope of the $\log j - \log F$ linear segments for our anthracene crystals cannot be simply attributed to sequential filling of either consecutive discrete ISW point individual traps or sets of traps distributed exponentially throughout the whole forbidden gap.

Now, we will demonstrate that the idea of macrotraps developed in Sections II.A and III.A satisfactorily explains the experimental results presented in Figure 3. The results are summarized in Table II.

The results presented in Table II show that the total energy of a hole in the macrotrap is the sum of the two terms as given by (cf. Figure 4).

$$E(r) = \begin{cases} \dfrac{3kT}{\sigma_1} \ln \dfrac{r_{o1}}{r} & \text{for} \quad r_{o1} \geq r \geq r^1 \\ \dfrac{3kT}{\sigma_2} \ln \dfrac{r_{o2}}{r} & \text{for} \quad r^1 \geq r \geq r_b, \end{cases} \tag{35}$$

where r^1 is a distance for which $(3kT/\sigma_1) \ln (r_{o1}/r^1) = (3kT/\sigma_2) \ln (r_{o2}/r^1)$, and $r_{o1} = r_o$. Since, however, in most the experimental cases both terms have been observed, it is useful to define the macrotrap extension r_2 at $E(r = r_2) = E_2$, where the both terms are equal each other (note that we used this definition for calculating r_2; see column ⑥ in Table II). Having determined r_2, E_2 can be evaluated from

TABLE II

Trapping parameters as determined from applying the discrete model macrotraps described in Section II.A and III.A.

Parameter	σ_1	σ_2	r_{o1} [Å]	E_t [eV]	r_{o2} [Å]	r_2 [Å]	r_b [Å]	E_t [eV]	E_t [eV]	N_{eff} [cm^{-3}]	$s=\pi r_{o1}^2$ [cm^2]	ν_{th} [s^{-1}]
Crystal	①	②	③	④	⑤	⑥	⑦	⑧	⑨	⑩	⑪	⑫
$d=49\mu m$	1.00	0.26	711	0.55	229	60	30	0.57	0.6	6.7×10^{14}	9.5×10^{-11}	1.3×10^{12}
$d=66\mu m$	0.90	0.33	550	0.55	456	201	35	0.57	0.6	1.4×10^{15}	1.6×10^{-10}	9.9×10^{11}

①, ② Taken from the slopes (n) of suitable segments (I and II) in Fig. 3. According to (26) $n = 2 + 3/\sigma$.

③ Calculated from (33) at transition voltage α (see Fig. 3), using ①.

④ Obtained from (26), using ③ and ① or ②, and making the assumption $N_{eff} = N_o$.

⑤ Obtained from (26) with ②, using ④.

⑥ Calculated from (3) at transition voltage β by equating $(3kT/\sigma_1)\ln(r_{o1}/r_2) = (3kT/\sigma_2)\ln(r_{o2}/r_2)$.

⑦ Calculated from (3), using ② and ④.

⑧, ⑨ Obtained from equating ΔE_H (11) to E_t and substituting, respectively, first σ_1 and r_{o1}, and then σ_2 and r_{o2} ($\vartheta = 0$ in both cases). In the calculation, the field (F) corresponding to the crossing point between Child's law curve and suitable extrapolated segments of the experimental curve has been substituted in (11).

⑩ Calculated from (4) assuming $N_{eff} = N_o$ and $H_o = N_m$, and using ③.

⑪ Obtained with values of r_{o1} as given in ③.

⑫ Calculated according to (27) with the assumption $N_{eff} = N_o$, $\nu = 10^7$cm/s, and using ⑪.

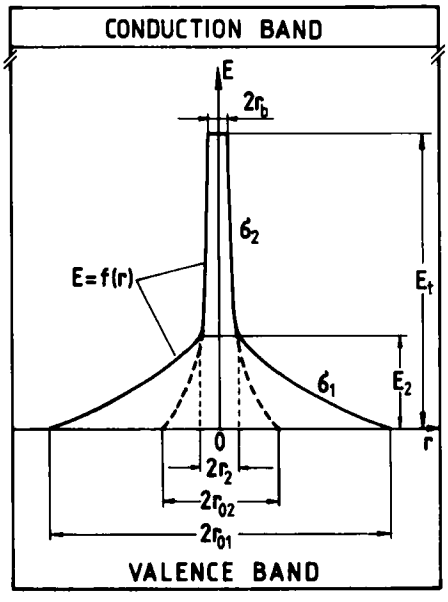

FIGURE 4 A two-dimensional representation of the potential well of the macrotraps in solution-grown anthracene crystals. For details see text.

Downloaded by [Tomsk State University of Control Systems and Radio] at 11:56 19 February 2013

Equation (3). This transition energy changes, in general, from crystal to crystal and in the case of our examples described in Table II takes the following values: $E_2(d = 49\mu m) = 0.18eV$ and $E_2(d = 66\mu m) = 0.08eV$. They constitute each less than one third of E_t.

The key difference between the standard SCLC *j-U* characteristic interpretation and that resulting from the presented macrotrap model is illustrated in Figure 5. While in the first case the nonlinear part of the plot follows the position of the quasi-Fermi level sweeping consecutive trap levels, in the second case it is due to lowering of the barrier with the quasi-Fermi level moving below the trapping level. The voltage at which a sudden increase in the current occurs, formerly referred to as the trap-filled-limit voltage or possible as to a step-increased value of *l* voltage, now corresponds to a step change in the macrotrap potential gradient with decreased σ.

We note that the calculation of the reduction of the barrier height as given in Sect. II A is a one-dimensional calculation. It overestimates the effective reduction in the barrier height, for only in the direction of the applied field is the edge of the potential well lowered as much as given by equations (11) and (12) with $\vartheta = 0$. A calculation of the effective reduction in barrier height by averaging the prob-

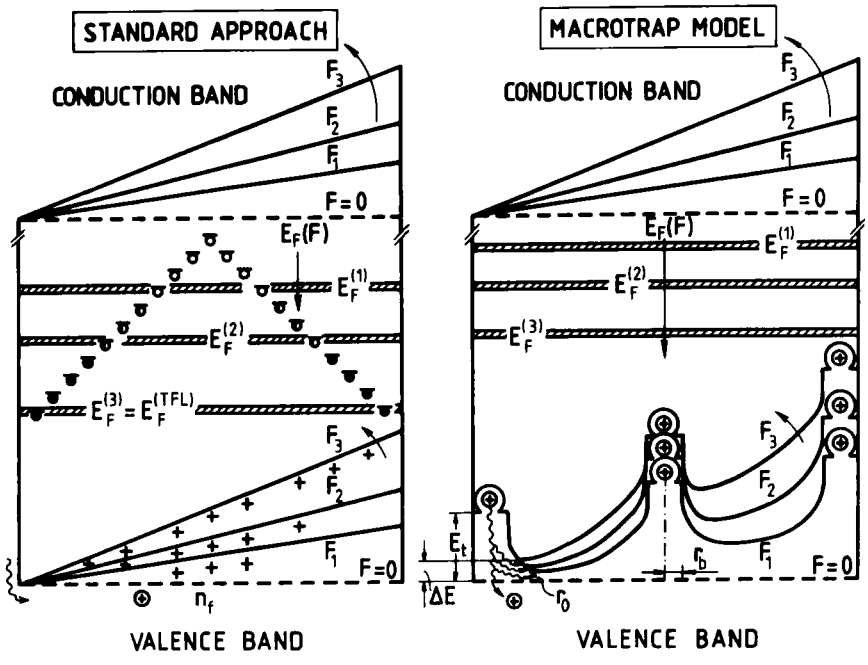

FIGURE 5 Comparison of standard and macrotrap model approaches to field-increasing hole current. $E_F^{(1)}$, $E_F^{(2)}$, $E_F^{(3)}$ correspond to consecutive positions of the quasi-Fermi level following increasing values of the applied field $F(1,2,3)$. $E_F^{(TFL)}$ is the position for the trap-filled-limit. "0" denotes the situation in the absence of the external electric field. In the macrotrap model approach a view of macrotrap potentials is shown (cf. Figure 4). The wavy lines illustrate thermal releasing of a hole from a macrotrap for increasing electric field.

Downloaded by [Tomsk State University of Control Systems and Radio] at 11:56 19 February 2013

Downloaded by [Tomsk State University of Control Systems and Radio] at 11:56 19 February 2013

ability of escape from the trap with respect to direction gives an increase in the concentration of free carriers which can be less by an order magnitude than that given in one-field oriented-dimension.[34] The experimental results obtained by us with over 20 solution-grown anthracene crystals show the trap parameters $\sigma_1 = 1.0 \pm 0.2$, $\sigma_2 = 0.30 \pm 0.05$ and $E_t = 0.60 \pm 0.05$ eV to be well reproducible from crystal to crystal, but the macrotrap radius varying between 100 and 10^3Å. As the macrotrap depth increases with r_o according to $E(r_o) = (3kT/\sigma)\ln(r_o/r_b)$ [see Equation (3)], it is possible to reconcile this apparent discrepancy by allowing for variation in the radius of the basal pinning trap r_b.

Thus it is not unreasonable to speculate that they constitute clusters of incipient dimers of varying sizes formed preferentially at dislocations as it has already been suggested earlier.[35] The values of $r_b \approx 30-40$Å (see Table II) seem to be reasonable sizes for small clusters of the dimers which are expected to involve a few pairs of molecules. Such dimer clusters distort the lattice in a certain region, producing and/or aggregating defects with energy states distributed in space according to a decreasing function given for instance by Equation (35). However, the macrotrap potential could be, in principle, considered as the strain energy in a dislocation itself. Based on distance (r) from the dislocation, two contributing terms of this energy are usually distinguished; for distances larger than r_2, there is $E^{(1)}(r)$, the elastic (continuum) strain energy, and for distances smaller than r_2 (but larger than r_b), one has $E^{(2)}(r)$, the core energy, which, in contrast to $E^{(1)}(r)$, cannot be evaluated from elastic approximation because the strains are too large.[36] The dimers created along dislocation lines would still form the pinning traps for the macrotraps. The radius r_o of a spherical macrotrap, which in this case is a term somewhat ill-defined, expresses the Burgers vector averaged distance at which the effect of the dislocation on intermolecular orientations and distances lies within kT of the effect of temperature on these parameters. The dislocation background of the macrotrap explains in a natural way two reproducible branches of the potential deduced from the experimental data (see Figure 4); the weak-gradient part ($\sigma_1 \approx 1$) due to weak strains created at distances larger than r_2, and strong-gradient part ($\sigma_2 \approx 0.3$) resulted from large strains located in the range $r_b < r < r_2$. The relatively large scatter of r_o and r_2 observed in experiment would reflect an anisotropy in magnitudes and orientations of the Burgers vector characterizing different dislocations. The dislocation interpretation of macrotraps is supported at last by their concentration which evaluated in our experiments at $\approx 10^{15}\text{cm}^{-3}$ falls in the range $10^{15}-10^{17}\text{cm}^{-3}$ as found in anthracene crystals by using etching techniques for localization of dislocations and then by their counting.[37] Since dislocations are typical extended faults arising in anthracene crystal lattice during crystal preparation and subsequent handling, one would expect them to be commonly observed with different techniques. The trap depths $E_t = 0.53-0.60$eV are indeed detected in anthracene crystals with TSC techniques (cf. References 38–40), but now for the first time the same values are found by the above analysis of steady-state SCLC j-U characteristics.

We note that the macrotrap-like concept has already been proposed in the past by Pope and coworkers (as quoted by Geacintov and Swenberg in Reference 41). They also used the notion of defect cages (the deformed regions of crystals around

Downloaded by [Tomsk State University of Control Systems and Radio] at 11:56 19 February 2013

defects) to explain the enhanced fluorescence quenching by injected charge carriers in anthracene crystals.

At this point we want to stress that our results summarized in Table II are self-consistent under the conditions $N_{\text{eff}} \cong N_o$ and $N_m \cong H_o$. They impose all molecules to be involved in formation of macrotraps, the macrotraps touch each other occupying approximately the whole volume of the crystal. This makes the carriers hopping from one to another macrotrap, the number of states available per 1cm^3 (N_{eff}) equals the density of macrotraps in contrast to the standard interpretation in which N_{eff} is usually identified with the molecular density N_m. [Note that $N_{\text{eff}} \approx N_m$ results directly from Equation (27) if for r_o the molecular dimension is substituted]. Since for our crystals the capacitor charge per unit area (CU/e) $< N_o$ within the entire range of the applied voltage, the TFL conditions for macrotraps cannot be fulfilled. In general, however, $N_{\text{eff}} > N_o$, $N_o <$ (CU/e), and TFL is attainable. This seems to be the case with naphthalene single crystal[20] for which the enormous discrepancy of about 5 orders of magnitude has been found in the trap concentration determined from the TFL voltage and from the temperature dependence of θ^2 for ISW point traps with $N_{\text{eff}} = N_m$.

Based on the macrotrap model this discrepancy can easily be resolved. The trap concentration $N_t(\text{TFL}) = 4.5 \times 10^{11}\text{cm}^{-3}$ obtained from the TFL voltage must be then identified with the concentration of macrotraps N_o but $N_t[\theta(T)] = 7.5 \times 10^{16}\ \text{cm}^{-3}$ obtained from the temperature dependence of θ according to Equation (31) is meaningless because of *a priori* assumed $N_{\text{eff}} = N_m$. Instead, $N_{\text{eff}} = 2.4 \times 10^{16}\text{cm}^{-3}$ results from (31) using $N_o = N_t(\text{TFL})$ and experimental values of θ. Hence, on the basis of (27) and (4) $r_o = 187\text{Å}$ and $H_o = 5 \times 10^{16}\text{cm}^{-3}$ can be calculated, respectively. We note that the sharp increase of the current in this case cannot be interpreted as the α-transition in sense of (33) since it leads to $N_o = 4.5 \times 10^9\ \text{cm}^{-3}$, the value much lower that $\text{CU}_{\text{tr}}/\text{e}$, that is TFL for these traps should appear at $U < U_{\text{tr}}$, which is not the case. Summarizing the results it must be pointed out that acting of discrete macrotraps can be seen in the shape of j-U characteristic only in high-perfection crystals for which $(N_o)^{-1/3} \geq 2r_{o1}$. In poor-quality crystals only two straight-line segments of $\log j - \log U$ plot should be observed; the second one with the slope $n > 2$ reflecting most probably a continuous energy distribution of microtraps dispersed homogeneously in space due to formation of macrotrap assemblies throughout the crystal (see Sect.II.B).

Interaction of macrotraps can lead then to softening of the core strains resulting in one averaged value of σ. This might also be the case of macrotrap distribution in energy, which, for $r_o = \text{const}$, lets the j-U dependence to be expressed by formula (34). This would, however, require r_b to be a decreasing function of E_t. Finally, despite the existence of well defined discrete macrotraps, the third segment may not occur because: (i) the voltage accessible in experiment is insufficient to lower the barrier down to place the maximum at $r_m \leq r_2$ (this is the case with $E_2 \rightarrow E_t$). From the slope of the second segment we can only derive σ_1; (ii) the applied voltage reduces the barrier within the transition range α to such an extent that at higher voltages $r_m < r_2$ (this is the case with $E_2 \rightarrow 0$), and then from the second segment slope we derive only σ_2. Whereas at present it is not possible to formulate a general rule how to distinguish between these different situations, one can arrive at a final

conclusion by a careful analysis of the particular experimental curve including, especially, the shape of the transition region α and evaluated from it r_{o1} and E_t.

In contrast, in high-perfection crystals one would expect at least three such segments suggesting the current to be controlled by a complex potential discrete macrotraps distributed randomly in space. The reason for the fourth segment (in Figure 3 $n = 3.4$ with the crystal of $d = 66\mu m$) is not yet established. It may be associated with a transition to the electrode-limited-current, but it is also possible that after filling the macrotraps each with one carrier, next trapping events proceed through the capture of the second carrier by the already charged macrotraps. The Coulombic repulsion of the two one-macrotrap located carriers makes the macrotraps to be shallower, which is demonstrated in the experiment as a decrease in the slope of the $\log j - \log U$ plot. In order to identify the process responsible for the current flow within this range a detailed analysis of various mechanisms has been undertaken by us and the results will be presented in a forthcoming paper.

Downloaded by [Tomsk State University of Control Systems and Radio] at 11:56 19 February 2013

Acknowledgment

This work was supported in part by the Polish Academy of Sciences under Program CPBP 01.14.

References

1. K. C. Kao and W. Hwang, "Electrical Transport in Solids (Pergamon Press, Oxford 1981).
2. M. Pope and C. E. Swenberg, "Electronic Processes in Organic Crystals" (Clarendon, New York 1982).
3. E. A. Silinsh, "Organic Molecular Crystals" (Springer, Berlin 1980).
4. A. Rose, *Phys. Rev.*, **97**, 1538 (1955).
5. J. Godlewski and J. Kalinowski, *Sol. State Commun.*, **25**, 473 (1978).
6. F. J. Bryant, A. Bree, P. E. Fielding and W. G. Schneider, *Disc. Faraday Soc.*, **28**, 48 (1959).
7. H. Kokado and W. G. Schneider, *J. Chem. Phys.*, **40**, 2937 (1964).
8. J. M. Thomas, J. O. Williams and G. A. Cox, *Trans. Faraday Soc.*, **64**, 2496 (1968).
9. M. Gamoudi, N. Rosenberg, G. Guilland, M. Maitrot and G. Mesnard, *J. Phys. C*, **7**, 1149 (1974).
10. G. M. Parkinson, J. M. Thomas and J. O. Williams, *J. Phys. C*, **7**, K310 (1974).
11. R. Eiermann, W. Hofberger and H. Bässler, *J. Non-Crystall. Solids*, **28**, 415 (1978).
12. F. Aramu, V. Maxia and G. Spano, *J. Lumin.*, **10**, 85 (1975).
13. F. Aramu, T. De Pascale, V. Maxia and G. Spano, *J. Lumin.*, **16**, 99 (1978).
14. W. C. Neely, K. Mandal and C. R. Peters, *J. Lumin.*, **29**, 341 (1984).
15. Z. Dreger and J. Kalinowski, "Abstracts Book of 11th Mol. Cryst. Symp." (Lugano, 1985), p. 64.
16. Z. Dreger and J. Kalinowski, *Mater. Sci.*, **13**, 51 (1987).
17. Z. Dreger and J. Kalinowski, Potsdamer Forsch., Reihe B, **Heft 52**, 16 (1987) (ISSN 0138-2454).
18. Z. Dreger, J. Kalinowski, I. Davoli, S. Stizza and S. Feliziani, *phys. stat. sol. (b)*, **149**, 363 (1988).
19. M. Schadt and D. F. Williams, *J. Chem. Phys.*, **50**, 4364 (1969).
20. M. Campos, *Mol. Crys. Liq. Cryst.*, **18**, 105 (1972).
21. P. J. Reucroft and F. D. Mullins, *J. Phys. Chem. Solids*, **35**, 347 (1974).
22. E. A. Silinsh, *phys. stat. sol. (a)*, **3**, 817 (1970).
23. J. Bonham, *Austral. J. Chem.*, **26**, 927 (1973).
24. S. Nespurek and E. A. Silinsh, *phys. stat. sol. (a)*, **4**, 747 (1976).
25. H. Bässler, *phys. stat. sol. (a)*, **107**, 9 (1981).
26. A. K. Jonscher, *Thin Solid Films*, **1**, 213 (1967).
27. P. C. Arnett and N. Klein, *J. Appl. Phys.* **46**, 1399 (1975).
28. B. M. Strunin, *Fiz. Tverd. Tela*, **9**, 803 (1967).
29. P. Mark and W. Helfrich, *J. Appl. Phys.*, **33**, 205 (1962).

30. W. Helfrich, in "Physics and Chemistry of the Organic Solid State," edited by D. Fox, M. M. Labes and A. Weissberger (Interscience Publishers, 1967), p. 1.
31. R. I. Frank and J. G. Simmons, *J. Appl. Phys.*, **38**, 832 (1967).
32. P. N. Murgatroyd, *J. Phys. D: Appl. Phys.*, **3**, 151 (1970).
33. P. J. Reucroft and F. D. Mullins, *J. Chem. Phys.*, **58**, 2918 (1973).
34. J. L. Hartke, *J. Appl. Phys.*, **39**, 4871 (1968).
35. M. Pope and H. Kallmann, *J. Israel Chem. Soc.*, **10**, 269 (1972).
36. Reference 2, p. 228.
37. G. P. Owen, J. Sworakowski, J. M. Thomas, D. F. Williams and J. O. Williams, *J. Chem. Soc. Far. II*, **70**, 853 (1974).
38. M. Schadt and D. F. Williams, *J. Chem. Phys.*, **50**, 4364 (1969).
39. J. S. Bonham, L. E. Lyons and D. F. Williams, *J. Chem. Phys.*, **56**, 1782 (1972).
40. S. Maeta and K. Sagakuchi, *J. Electronics (Jpn)*, **98**, 33 (1977).
41. N. E. Geacintov and C. E. Swenberg, in: "Organic Molecular Photophysics," Vol. 2, edited by J. B. Birks, Wiley & Sons, 1975. p. 400.

Downloaded by [Tomsk State University of Control Systems and Radio] at 11:56 19 February 2013